Capacity estimation of beam-like structures using Substructural Method

Shojaeddin Jamali,[1] Tommy HT Chan,[2] Ki-Young Koo,[3] Andy Nguyen,[4] and David P Thambiratnam[5]

[1]Ph.D. Candidate, Department of Civil Engineering and Built Environment, Queensland University of Technology. Email: shoja.jamali@qut.edu.au

[2] Professor, Department of Civil Engineering and Built Environment, Queensland University of Technology. Email: Corresponding author: tommy.chan@qut.edu.au

[3] Lecturer, Vibration Engineering Section, College of Engineering, Mathematics and Physical Sciences, University of Exeter, Exeter EX4 4QF, UK. Email: K.Y.Koo@exeter.ac.uk

[4] Lecturer, School of Civil Engineering and Surveying, University of Southern Queensland. Email: Andy.Nguyen@usq.edu.au

[5] Professor, Department of Civil Engineering and Built Environment, Queensland University of Technology. Email: d.thambiratnam@qut.edu.au

Abstract. Evaluating the performance of beam-like structures in terms of their current boundary condition, stiffness and modal properties can be challenging as the structures behave differently from their designed conditions due to aging. The purpose of the current study is to determine the flexural rigidity of beam-like structures when their support conditions are not fully understood. A novel optimization scheme is proposed for estimation of the flexural stiffness and the capacity of the beam-like structures under moving loads. The proposed method is applied to various profiles of the beams made of different materials with unknown boundary condition, and the effects of damage, excitation and optimization algorithm are rigorously investigated. The results of the numerical and experimental studies showed that the proposed substructural bending rigidity identification (SBI) method can correctly assess the in-service flexural stiffness, fixity of the boundary condition, and the load carrying capacity. This technique can be considered as a cost-effective method for periodic monitoring, load rating, and model updating of the beam-like structures.

Keywords: Stiffness, beam, substructural, load carrying capacity, structural health monitoring, load rating.

1. Introduction

Recent trends in structural health monitoring (SHM) have led to a proliferation of studies that assess the beam-like structures using vibrational characteristics such as natural frequency and mode shape.[1-3] In addition, many performance assessments using dynamic methods have been stipulated for various standards, such as fatigue assessment in the national bridge design code, or vibration-based damage detection in AS5100 Part 7.[4] Bending stiffness plays a critical role in the assessment of beam-like structures, since the predominant failure mode for such elements is bending. Flexural rigidity can be viewed as an indicator of system stiffness and structural integrity that is related to the load carrying capacity (LCC). Previous studies conclusively showed that the LCC of the bridge decreases over time, due to various factors such as environmental conditions, over-loading, and material deterioration.[5, 6]

A detailed review on stiffness identification methods by Hoffmann *et al.,*[7] demonstrated that global stiffness needs to be efficiently measured for assessment of aging structures. Subramaniam[8] and Chowdhury[9] reported that using the load-displacement relationship and the single degree of freedom (DOF) system, static stiffness can be obtained. Similar studies evaluated the flexural rigidity and LCC of beam-like structures using Euler beam theory and serviceability deflection limits.[10-15] These studies have not treated the support conditions in much detail, and the bridge was typically simplified as a simply supported beam with concentrated load at mid-span. The fixity of the boundary conditions in bridge, such as at abutments changes throughout service life; hence, estimating the support condition based upon design documents does not reflect the true boundary condition.[16] It is well established that the support conditions directly affect the load path and the deformation of the structure. This paper proposes the Substructural Bending Rigidity Identification (SBI) method for evaluating the bending stiffness and boundary condition of beam-like structures. SBI adopts divide and conquer strategy, which has been used for system identification of various structural elements.[17-20] SBI method splits the structure into several substructures for identification of the structural parameters, and effectively reduces the unknown DOFs and ill-conditioned problems in the structural system identification. For verification, a combination of numerical and experimental analyses is used to investigate the applicability of the proposed method.

2. Theoretical Development

Real civil structures have many DOFs and thus analysing every one of them as the whole is very challenging. The fundamental concept in SBI is that the response of the internal substructure is related to the interfacial response of substructural length. As shown in Fig. 1, a continuous bridge deck is divided into a series of internal substructures, independent of boundary conditions and other spans. For each respective substructure, global stiffness is estimated by minimizing the error norm between the vertical and the rotational acceleration responses, with that of vertical acceleration in the mid-region of the substructure.
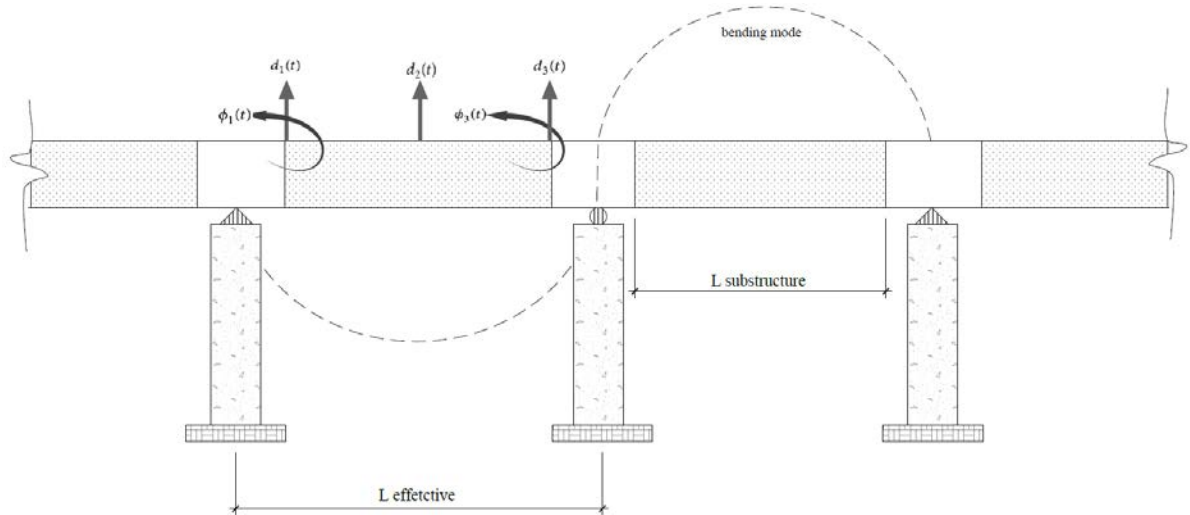

Fig. 1. SBI layout of substructural system for input-output relationship.

According to the Euler-Bernoulli beam theory, the governing equation for dynamic beam would be:

$$EI \frac{\partial^4 y}{\partial x^4} = -\mu \frac{\partial^2 y}{\partial t^2} + q \tag{1}$$

where μ is the product of mass density and cross sectional area. For a homogeneous beam, EI is constant, and in the absence of external loads, the free vibration equation becomes:

$$\left[\frac{EI}{\mu} \right]^2 \frac{\partial^4 y}{\partial x^4} + \frac{\partial^2 y}{\partial t^2} = 0 \tag{2}$$

3

By using the separation of variables technique, the displacement function for the forced and the free vibration is defined as:

$$y(x,t) = X(x)T(t) \tag{3}$$

Rearranging Eq. (3) to (2):

$$\frac{[EI/\mu]^2}{X(x)} \frac{\partial^4 X(x)}{\partial x^4} = \frac{-1}{T(t)} \frac{\partial^2 T(t)}{\partial t^2} = \omega^2 \tag{4}$$

where ω is defined as a constant. Equation (4) can be expressed in terms of two ordinary differential equations as:

$$\frac{\partial^4 X(x)}{\partial x^4} - \lambda^4 X(x) = 0 \tag{5}$$

$$\frac{\partial^2 T(t)}{\partial t^2} + \omega^2 T(t) = 0 \tag{6}$$

$$\text{Where} \quad \lambda^4 = \frac{\rho A \omega^2}{EI} \tag{7}$$

The general solution of Eq. (5) and (6) is given by:

$$X(x) = C_1 \sinh(\lambda x) + C_2 \cosh(\lambda x) + C_3 \sin(\lambda x) + C_4 \cos(\lambda x) \tag{8}$$

$$T(t) = C_5 \sin(\omega t) + C_6 \cos(\omega t) \tag{9}$$

Where C_1 to C_6 are termed as constants. Substituting above equations into the general displacement function:

$$y(x,t) = \begin{bmatrix} \sinh(\lambda x) & \cosh(\lambda x) & \sin(\lambda x) & \cos(\lambda x) \end{bmatrix} C e^{i\omega t} \tag{10}$$

For $C = [C_1 \ C_2 \ C_3 \ C_4]^T$, the end conditions of the beam are:

$$\begin{cases} v(0,t) = d_1(t) & v(L,t) = d_3(t) \\ \left. \dfrac{\partial v(x,t)}{\partial x} \right|_{x=0} = \phi_1(t) & \left. \dfrac{\partial v(x,t)}{\partial x} \right|_{x=L} = \phi_3(t) \end{cases} \tag{11}$$

The solution of (11) is found as a linear algebraic equation using interfacial boundary conditions as:

$$\begin{bmatrix} 0 & 1 & 0 & 1 \\ \lambda & 0 & \lambda & 0 \\ \sinh \lambda L & \cosh \lambda L & \sin \lambda L & \cos \lambda L \\ \lambda \cosh \lambda L & \lambda \sinh \lambda L & \lambda \cos \lambda L & -\lambda \sin \lambda L \end{bmatrix} \mathbf{C} e^{i\omega t} = \begin{bmatrix} d_1(t) \\ \phi_1(t) \\ d_3(t) \\ \phi_3(t) \end{bmatrix} \tag{12}$$

When the right-hand side and left-hand side matrix are set as $U(t)$ and A, then a solution can be obtained by substituting $\mathbf{C}e^{i\omega t}$ with $\mathbf{A}^{-1}\mathbf{U}(t)$ as:

$$y(x,t) = \left[\sinh(\lambda x) \ \cosh(\lambda x) \ \sin(\lambda x) \ \cos(\lambda x) \right] A^{-1} U(t) \tag{13}$$

$U(t)$ is a column vector and has input displacement at both interfacial boundaries of the beam. To obtain the transfer function for interfacial boundaries, the Fourier transform is applied to both sides of (13) with respect to displacement. Thus, the transfer function can be defined as:

$$H(\omega) = \frac{\text{output response @ internal substrcture}}{\text{input response @ interfacial boundaries}} \tag{14}$$

The input responses are vertical and rotational accelerations near the boundary conditions (two on each side), while the output response is the vertical acceleration in the mid-span. Using Fourier transform principles, (13) becomes:

$$H(x,\omega) = \left[\sinh(\lambda x) \ \cosh(\lambda x) \ \sin(\lambda x) \ \cos(\lambda x) \right] A^{-1} \tag{15}$$

$$U(\omega) = \left[d_1(\omega) \ \phi_1(\omega) \ d_3(\omega) \ \phi_3(\omega) \right]^T \tag{16}$$

where $d_1(\omega)$ and $d_3(\omega)$ are the vertical accelerations; $\phi_1(\omega)$ and $\phi_3(\omega)$ are the rotational accelerations.

Transfer function for the center of the substructure is taken at $x = L/2$ and can be derived as:

$$H(\omega)_{x=L/2} = \begin{bmatrix} h_1(\omega) & h_2(\omega) & h_3(\omega) & h_4(\omega) \end{bmatrix} \tag{17}$$

$$h_1(\omega) = h_3(\omega) = \frac{1}{2} \cdot \frac{\sin\left(\dfrac{\lambda L}{2}\right) + \sinh\left(\dfrac{\lambda L}{2}\right)}{\sin\left(\dfrac{\lambda L}{2}\right)\cosh\left(\dfrac{\lambda L}{2}\right) + \cos\left(\dfrac{\lambda L}{2}\right)\sinh\left(\dfrac{\lambda L}{2}\right)} \tag{18}$$

$$h_2(\omega) = -h_4(\omega) = \frac{-1}{2\lambda L} \cdot \frac{\cos\left(\dfrac{\lambda L}{2}\right) - \cosh\left(\dfrac{\lambda L}{2}\right)}{\sin\left(\dfrac{\lambda L}{2}\right)\cosh\left(\dfrac{\lambda L}{2}\right) + \cos\left(\dfrac{\lambda L}{2}\right)\sinh\left(\dfrac{\lambda L}{2}\right)} \tag{19}$$

Equation (17) is further simplified by using the non-dimensional variable ξ:

$$H(\xi) = \begin{bmatrix} \overline{h_1}(\xi) & L\overline{h_2}(\xi) & \overline{h_3}(\xi) & L\overline{h_4}(\xi) \end{bmatrix} \tag{20}$$

$$\xi = \frac{\lambda L}{2} = \sqrt[4]{\frac{\rho A}{EI}}\frac{\sqrt{\omega}L}{2} \tag{21}$$

$$\overline{h_1}(\xi) = \overline{h_3}(\xi) = \frac{1}{2} \cdot \frac{\sin(\xi) + \sinh(\xi)}{\sin(\xi)\cosh(\xi) + \cos(\xi)\sinh(\xi)} \tag{22}$$

$$\overline{h_2}(\xi) = \overline{h_4}(\xi) = \frac{-1}{4\xi} \cdot \frac{\cos(\xi) - \cosh(\xi)}{\sin(\xi)\cosh(\xi) + \cos(\xi)\sinh(\xi)} \tag{23}$$

The relationship between the center output $[d_2(\omega)]$ and the interfaces input of the substructure can be represented as:

$$d_2(\omega) = H(\xi)\begin{bmatrix} d_1(\omega) & \phi_1(\omega) & d_3(\omega) & \phi_3(\omega) \end{bmatrix}^T \tag{24}$$

$$= \overline{h_1}(\xi)d_1(\omega) + L\overline{h_2}(\xi)\phi_1(\omega) + \overline{h_3}(\xi)d_3(\omega) + L\overline{h_4}(\xi)\phi_3(\omega)$$

Equation (24) is further simplified by considering the relationship in (23) and (22):

$$d_2(\omega) = \overline{h_1}(\xi)\big(d_1(\omega) + d_3(\omega)\big) + L\overline{h_2}(\xi)\big(\phi_1(\omega) - \phi_3(\omega)\big) = \overline{h_1}(\xi)u_1(\omega) + L\overline{h_2}(\xi)u_2(\omega) \quad (25)$$

$$u_1(\omega) \,\square\, d_1(\omega) + d_3(\omega) \ \text{ and } \ u_2(\omega) \,\square\, \phi_1(\omega) - \phi_3(\omega) \tag{26}$$

For analysis, the spectral densities are obtained for (25):

$$\lim_{T\to\infty}\frac{1}{T}d_2^*(\omega)d_2(\omega) = \overline{h_1}(\xi)\lim_{T\to\infty}\frac{1}{T}d_2^*(\omega)u_1(\omega) + \overline{h_2}(\xi)L\lim_{T\to\infty}\frac{1}{T}d_2^*(\omega)u_2(\omega)$$

$$\overset{yields}{\longrightarrow} \qquad S_{yy}(\omega) = \overline{h_1}(\xi)S_{1y}(\omega) + \overline{h_2}(\xi)LS_{2y}(\omega) \tag{27}$$

where $S_{yy}(\omega)$ is the power spectral density (PSD) and is calculated using the response at the center of the substructure, while $S_{1y}(\omega)$ and $S_{2y}(\omega)$ are the cross-spectral densities (CSD) obtained by four responses at the interfaces. The unknown parameter ξ is obtained by optimization of the responses in the interfaces and the center of the substructure using (28):

$$\min(\xi) = \int_{\Omega}\Big\{S_{yy}(\omega) - \big(\overline{h_1}(\xi)S_{1y}(\omega) + \overline{h_2}(\xi)LS_{2y}(\omega)\big)\Big\}^2 d\Omega \tag{28}$$

where Ω is the domain of integration in the first flexural mode. With reference to (21), global stiffness of the beam is estimated as:

$$EI_{SBI} = \frac{\rho A\omega_1^2 L_{sub}^4}{16\xi^4} \tag{29}$$

where $\omega_1 = 2.\pi.f_1$ and L_{sub} is the substructural length used for optimization. To minimize the difference of the input-output responses, a nonlinear curve square fitting method is used due to its fast and robust convergence.

7

Estimated bending stiffness acts as a sensitive indicator of the physical change, whereby any reduction in the stiffness makes the structure more flexible, and causes loss of the bearing capacity. It can be assumed that the global stiffness is proportional to the fundamental frequency, whereas static deflection is inversely proportional to the global stiffness. As such, 10% drop of the stiffness causes 5% reduction in the fundamental frequency of the beam and 11% increases in the static deflection of the mid-region.[21] Therefore, the health of the structure is associated with its dynamic response, and any distress can be fairly estimated from the vibrational signature of the structure. Since the first bending structural mode dominates both static and dynamic responses of a bridge simplified as a beam[22], then the bending mode for that structure attracts the highest portion of energy. Estimated global stiffness is substituted into Euler beam theory to estimate the fixity of the boundary condition using Eq. (30).

$$f = \frac{\lambda^2}{2\pi L_{effective}^2}\sqrt{\frac{EI_{SBI}}{m}} \tag{30}$$

The first bending frequency ($f = f_1$) is obtained from measurements when optimizing (ξ) in Eq. (28); L is the effective length of the beam, not to be confused with (L_{sub}) for SBI optimization. After finding (λ), the true boundary condition of the beam can be back-calculated by referring to the natural frequencies and mode shapes of the beam. Fig. 2 shows the boundary coefficients (λ) that are computed using boundary condition restraints for fundamental frequency of a single span beam.[23] The process of SBI is summarized in Fig. 3 using the responses of the interfacial and the internal substructure.
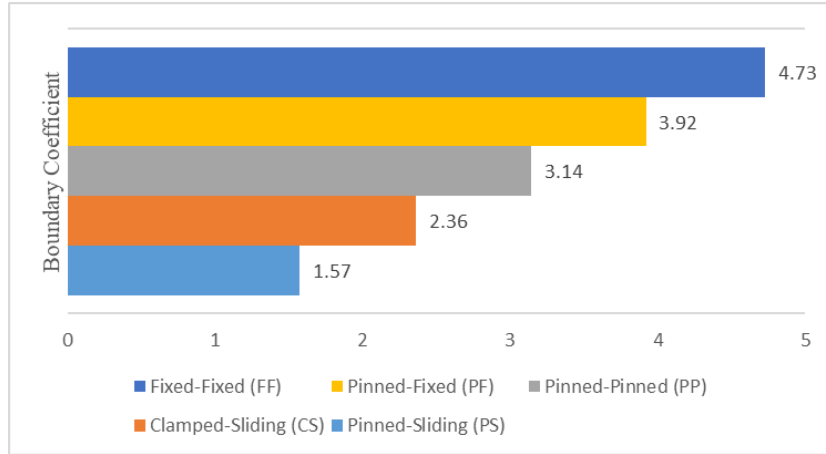
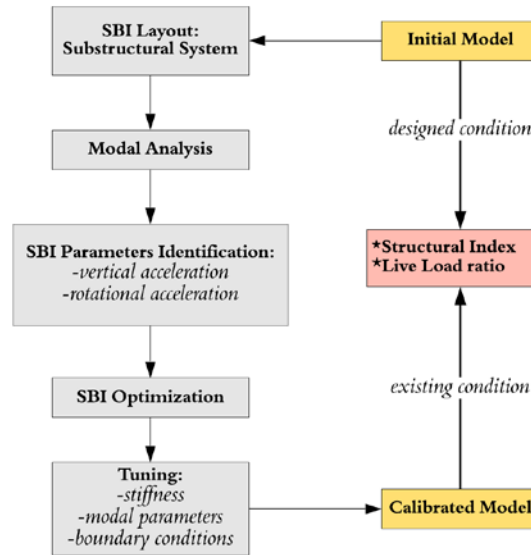Fig. 2. Boundary coefficients of single span beam.

Fig. 3. Process of SBI.

Estimated stiffness by the SBI method is related to the load capacity using a two-criterion approach — structural index and live load ratio.

$$\text{Structural Index} = \frac{EI_{SBI}}{EI_{Intact}} \tag{31}$$

$$\text{BM}_{LL} = \frac{\phi M_{ULS} - \gamma_{DL} M_{DL} - \gamma_{SDL} M_{SDL}}{\sum_{i=1}^{n} \gamma_{LL} M_{LL}(1 + DLA)*A V F}, \quad \text{SF}_{LL} = \frac{\phi V_{ULS} - \gamma_{DL} V_{DL} - \gamma_{SDL} V_{SDL}}{\sum_{i=1}^{n} \gamma_{LL} V_{LL}(1 + DLA)*A V F} \tag{32}$$

The structural index in Eq. (31) explicitly defines the capacity due to variations in the global bending stiffness, because any reduction in the bending stiffness of the beam-like structures reduces the resistance capacity. Intact bending stiffness (EI_{Intact}) is the designed stiffness based on the design information, while EI_{SBI} is the existing stiffness obtained from SHM testing using SBI method. The live load ratio analytically evaluates the capacity using an updated numerical model in terms of bending moment (BM) and shear force (SF) ratios. In Eq. (32), ϕM_{ULS} is the factored ultimate capacity, M_{DL} is the dead load moment, M_{SDL} is the superimposed dead load moment, M_{LL} is the live load moment due to the assessment vehicles, DLA is the dynamic load allowance, γ is the load factor, and AVF is the accompanying vehicle factor. Parameters for SF live load ratio are calculated similarly. Live load ratio greater than 1 indicates that the available capacity for the nominated loading is sufficient.

3. Implementation and Results

This section examines the effectiveness of the SBI method by providing a series of verification studies conducted numerically and experimentally.

3.1 Multi-span Reinforced Concrete Beam

Numerical simulation is carried out on a three-span rectangular reinforced concrete beam. The configuration of the beam is shown in Fig. 4, with an effective length (L_{eff}) being the center-to-center spacing of each span (8m), while substructure (L_{sub}) is the center-to-center spacing of the sensors (7.2m), and (L_{sen}) is the distance between two adjacent sensors (0.5m).

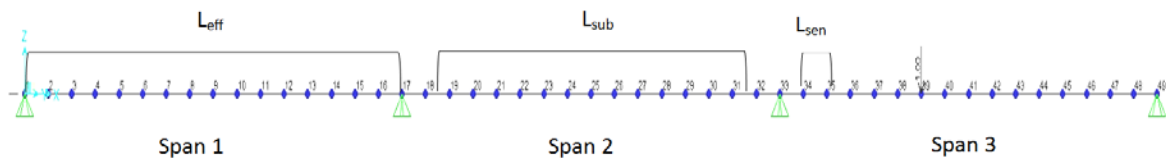Fig. 4. Configuration of the continuous beam.

Sectional properties of each span are I = 1.067 $\times 10^{-3}$ m^4, E = 24855578 $\times 10^3$ N/m^2, A = 0.08 m^2 and p= 23.57 kN/m^3. Excitation was induced as a Gaussian random load at span 3 and for each span, measurements were recorded at the mid and the end of L_{sub} span.

Due to the location of the measurement points, some natural frequencies could not be captured. However, if the first bending mode is detected, other modes of vibration are not needed for optimization. It is apparent from Fig. 5 that apart from the first bending mode, other detected frequencies are not in the same order. Low-pass filtering is applied to isolate the first bending mode for SBI optimization.
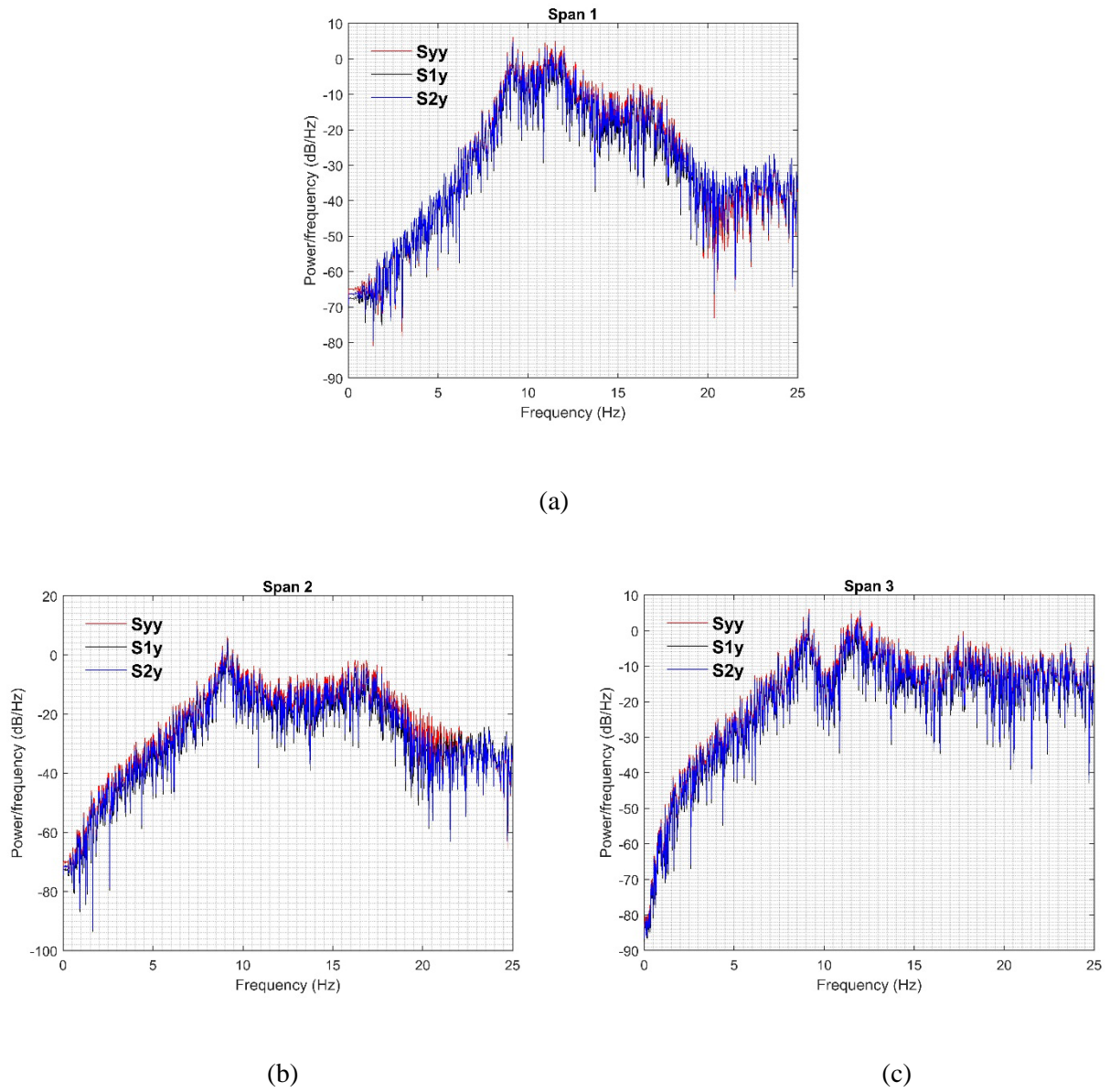

(a)

(b)

(c)

Fig. 5. Spectral amplitudes: (a) span, (b) span 2, (c) span 3

Average global stiffness was found to be 2.683×10^7 N.m^2, which gives a structural index equal to unity. Using Eq. (30) and with reference to Fig. 2, support fixity is estimated as the PP condition ($\lambda = 3.13$).

Identified modal parameters, boundary condition, and stiffness are used to update the numerical model. Applying Eq. (32) to the updated model, the flexural capacity of the beam under a wheel load of 8 kN is estimated as 2.6, while the shear capacity is estimated as 1.85; which indicates that the beam has sufficient capacity for this loading condition. In the case of a non-uniform cross-section with a varying second moment of area, an equivalent second moment of area taken at one-fifth of the interior span from interior support is considered.[24] If the beam in Fig. 4 is replaced by a haunch cross section, an equivalent second moment of area is taken at (0.2 L_{eff}) of the interior span.[25] An implication of this would be for assessment of the critical girders in continuous beam-like structures to provide insights into the load distribution and the stiffness of the girders.

3.2   T-beam Bridge

Application of the SBI method for bridge girder is investigated using a single span reinforced concrete T-beam bridge, a common type of bridge configuration found on country roads of Australia (Fig. 6).
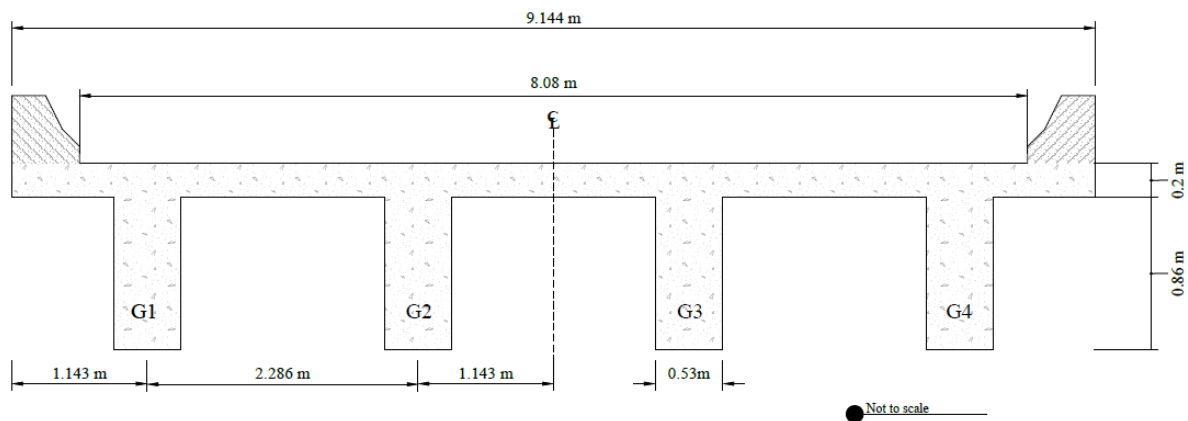

Fig. 6. Cross-section view of the deck.

The bridge has four 15.2m girders that rest on abutments via elastomeric bearing at their ends. Data was collected at the 4th girder (G4) using SM1600 vehicles as defined in AS 5100.2 for two lanes.[26]

Convergence of the minimization function in the optimization can be seen in Fig. 7. It is apparent that the differences of the interfacial (*S1y-S2y*) responses are minimized with respect to the output response at the center of the girder *(Syy)*, and this also confirms the stabilized convergence of the optimization function.
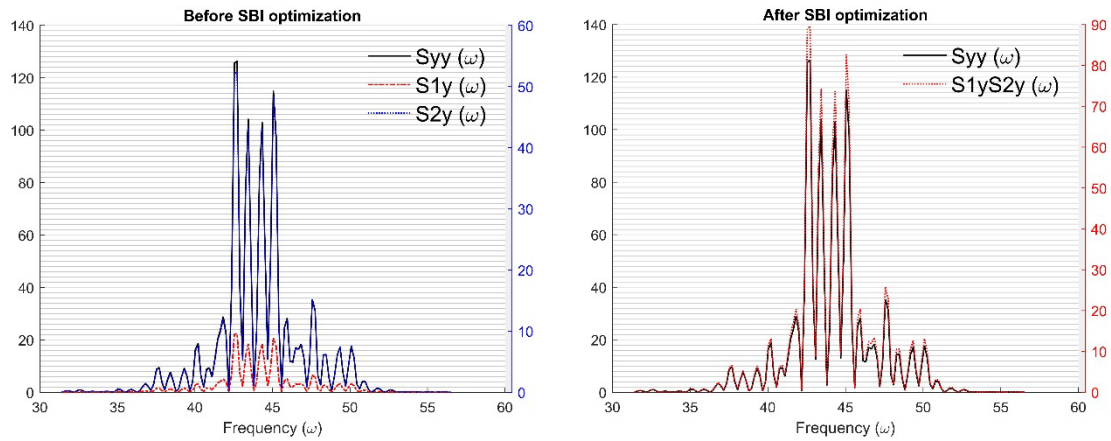
Fig. 7. Minimization of bending peak prior and after SBI optimization.

Using the SBI method, global stiffness of the girder is estimated as 8.372×10^9 N.m^2, which gives a structural index of 0.88 when compared with the intact stiffness. Reduction in the structural index can be due to aging, operational and environmental factors. Following estimation of the stiffness and boundary condition ($\lambda = 3.06$), finite element model updating is conducted to calibrate the numerical model in the linear range. This was achieved by carrying out a sensitivity analysis between experimental and analytical parameters, e.g. sensitivity of the stiffness and boundary conditions to change in the natural frequencies. Based on the information gained from sensitivity analysis, model updating is performed using differential method to minimize the difference between experimental and numerical parameters.[27] Superstructure is assessed for two-lane operation of 10 and 50 km/hr travelling speeds for three different cases under 45.5t and 42.5t semi-trailers (see Fig. 8).[28] For the first case, the reference and accompanying vehicles are moving along the lane centreline; in the second case, one of the vehicles is 0.6m away from the edge of the kerb, while another vehicle is centrally positioned in the other lane. In third case, the reference vehicle is running in either lane without accompanying vehicle.
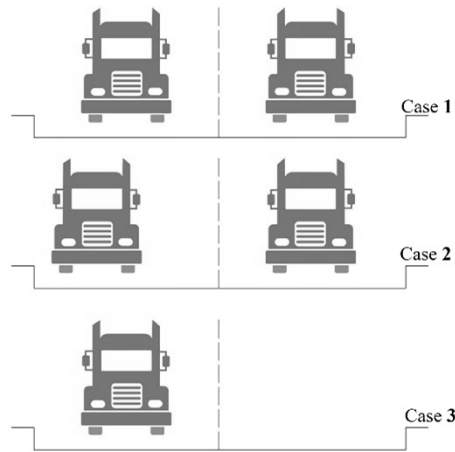
13

Fig. 8. Assessment vehicle positions.

It was found that the right exterior girder (G4) has the highest load effects when the reference vehicle was positioned in the right lane, and the accompanying vehicle was in the left lane at the speed of 50 km/hr. By applying Eq. (32), the live load bending moment ratio is 0.43, and the shear force ratio is 0.95. It can be stated that travel restrictions must be considered for this bridge, since G4 has no reserved capacity for assessed vehicular loadings. This result indicates that SBI is applicable for assessment of short to medium span bridges using ambient vibration with a minimum of 5 sensors, which can be considered in routine periodic inspections such as vibration-based assessment stipulated in AS 5100.7.[4]

3.3 *Steel Beam*

A steel beam was tested by using C-clamps at both ends with different pressure to simulate unknown boundary conditions (see Fig. 9). S1 and S2 are left-end sensors to record vertical and rotational accelerations, while S4 and S5 are right-end sensors, along with a central output response at S3. Sensors were affixed to the surface of the beam using instant adhesive gel. Random excitation was provided by modal hammer moving along the beam to simulate traffic excitation.
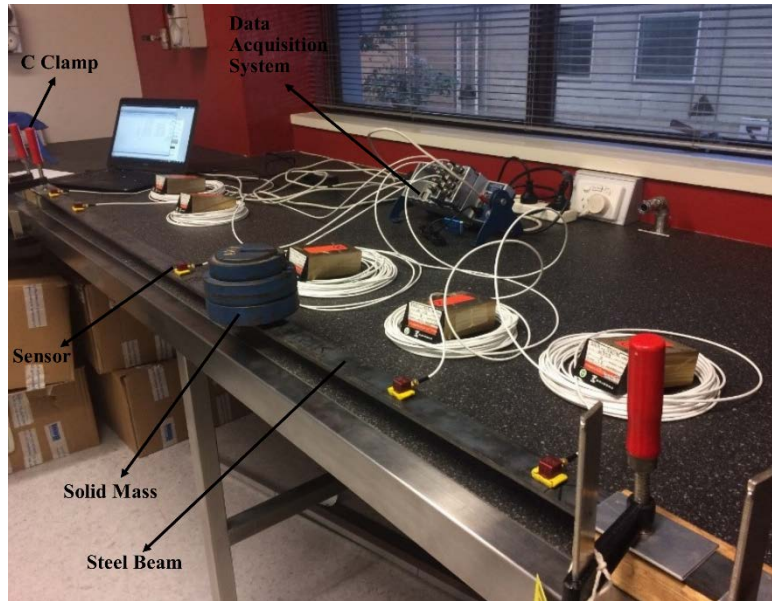
(a)
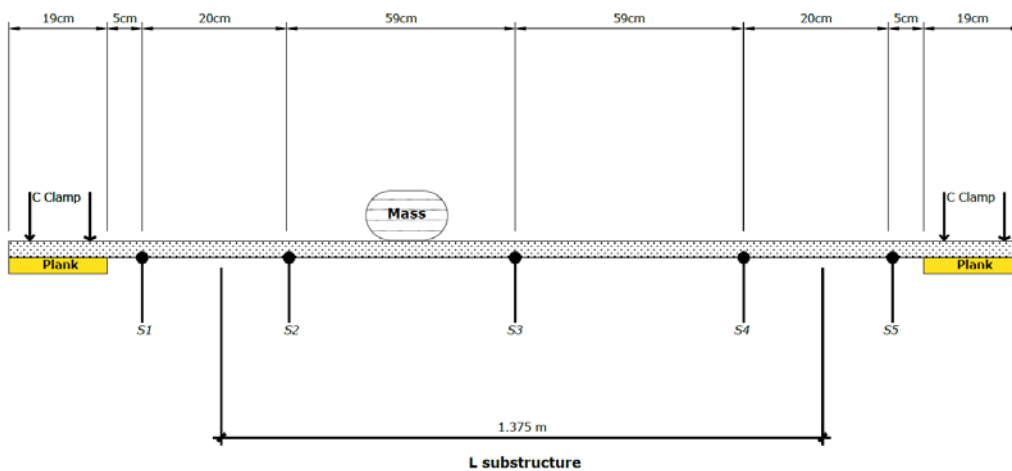
(b)

Fig. 9. (a) Testing condition of steel beam; (b) SBI testing setup.

Solid mass was added as shown in Fig. 9 to the beam by magnet to study the effect of damage on estimated stiffness. For each measured response, data was processed on-site to detect any change in the measured responses. This enabled detection and separation of spurious modes from real structural modes by comparing mode shapes across all measured datasets (see Fig. 10).
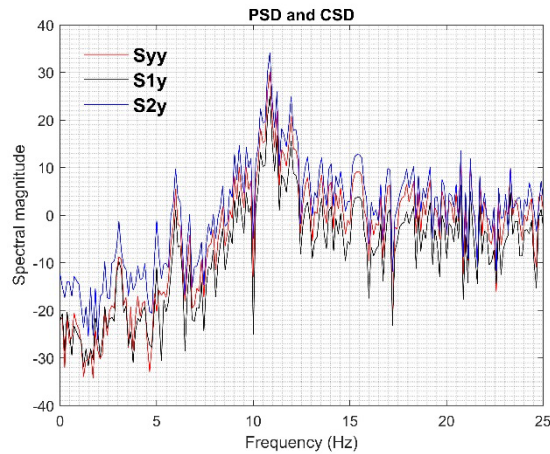
Fig. 10. Spectral amplitude of substructural system.

In Table 1, a clear trend of reduction is apparent in the bending frequency and the stiffness due to extra mass. From this data, correlation between stiffness and bending frequency to the change in the structural parameters can be observed, highlighting the sensitivity of these parameters to damage and the suitability of the SBI in detection of modal and structural parameters. For the steel beam, any reduction in the structural index is an indication of loss in the structural capacity, limited by yield stress or permissible deflection. In terms of damage assessment, other types of damage that occur throughout the life of the structure are not always severe, and difficult to be detected by global analysis such as steel reinforcement corrosion. To assess the localized damage, an updated numerical model coupled with existing methods for damage detection in the literature can be carried out for micro-scale analysis.[29] The findings of this experimental study suggest that the SBI method can monitor the state of change in the boundary condition, the bending stiffness and the structural capacity.

Table 1. Comparison of damaged states for steel beam.

Damage	Bending Frequency (Hz)	E ($\times 10^{11}$ N/m²)	ξ	Structural Index
Intact	10.9	2.2539	1.8402	1.0
0.5 kg	10.49	1.9344	1.8756	0.86
1 kg	9.86	1.7219	1.8721	0.76
2 kg	8.87	1.5494	1.8231	0.69
5 kg	7.65	1.4717	1.715	0.65

3.4 Prestressed Box Girder

In another experimental study, a laboratory-scale post-tensioned box girder was tested. As presented in Fig. 11(a), the 6m box girder is placed on supports at 100mm from its ends, and has two 15.2mm strands with a draped parabolic profile. Using random modal hammer tapping, measurements were recorded using piezoelectric sensors.
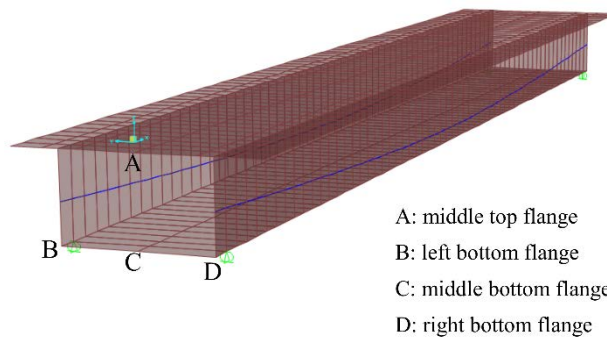
(a)   (b)

Fig. 11. (a) box girder in testing condition; (b) sensor locations for SBI.

For each location, data was post-processed using Fast Fourier and Welch methods.[30] Two algorithms were implemented for comparison; viz. 'trust-region-reflective'[31] and 'Levenberg-Marquardt' methods[32]. To minimize the effect of signal to noise ratio on the optimization function in the ambient

testing, numerous measurements were repeated for each testing location to ensure consistency in the recorded measurements. A comparison of the two results in Fig. 12 reveals that the first bending mode is correctly detected and the major difference is due to averaging of the signals in the Welch method, while Fast Fourier uses the full-length signal. This could be of importance when very closely spaced early frequencies are present in the structure, which makes the identification of the bending region for optimization less efficient.
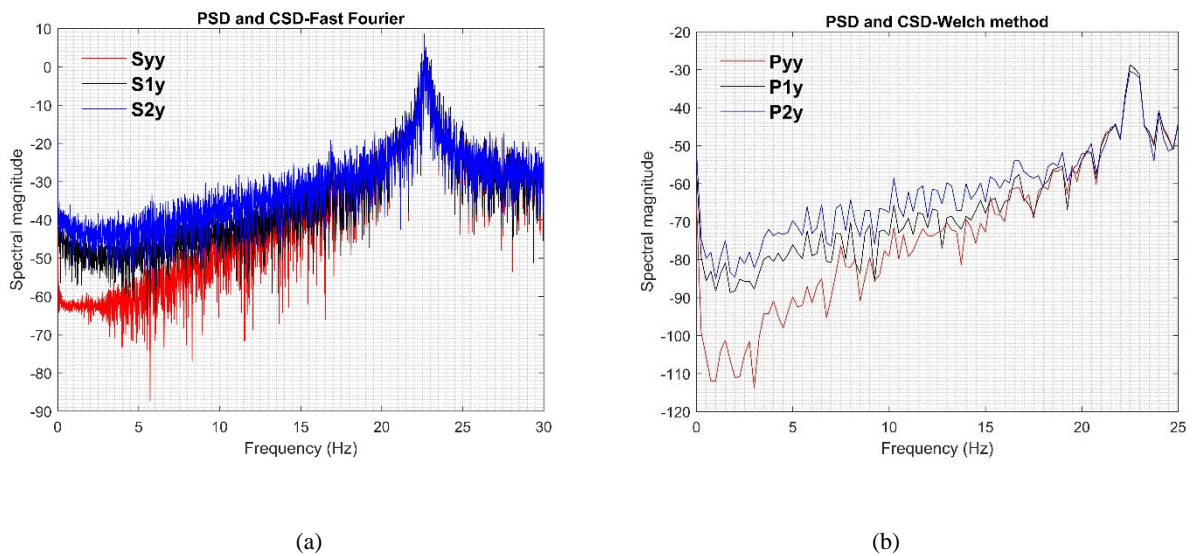

(a)   (b)

Fig. 12 (a) spectral amplitude using Fast Fourier; (b) spectral amplitude using Welch method.

Intact stiffness (EI = 1.419×10^8 N.m^2) was obtained by taking the average test results of several concrete core samples taken during the casting process. The structural index should be close to unity, since the box girder is relatively a new structure at the time of testing. As shown in Table 2, there is a significant difference between the estimated global stiffness at different locations.

Table 2. Comparison of SBI output for different locations

Location	Bending mode (Hz)	ξ (average)	EI (N.m^2)
A	22.65	1.1311	1.402×10^8
B	22.71	1.0528	1.868×10^8

C	22.71	1.2642	8.987×10^7
D	22.71	1.0915	1.615×10^8

High variations for the bottom portion of the box beam may be explained by the fact that the girder does not precisely represent the Euler beam which can be related to the modal data, in which the lower modes including the first mode were torsional and lateral modes, and not a flexural mode. Due to this, non-pure bending modes in the SBI optimization can cause a noticeable change in the error norm (ξ). Another source of the difference could be attributed to the post-tensioning, because the post-tensioning was completed in two stages and the data was logged after the final post-tensioning, causing the web and bottom flange regions to become too stiff. In contrast, the top flange (location A) had better estimation, mainly because of its deformation representing the pure bending mode and its slenderness. Moreover, it is possible that the results of the bottom portions have been affected by lack of precise rotational acceleration measurement. Spacing of the sensors for obtaining rotational acceleration at interfacial locations was set to 0.5m, which can bias the preciseness of the rotational acceleration estimated from the spacing of the two adjacent sensors at each end.

Using the updated numerical model, the box girder is load rated for A160 loading, based on AS5100.2.[26] The dimension and wheel loads of A160 (10%) are scaled down by a factor of 10 to match the carriageway of the box girder. Live load ratios resulted in 1.51 for flexural capacity, and 3.87 for shear capacity. This indicates that the box girder has reserved capacity, and so unrestricted travel is allowed for A160 (10%) loading. Both optimization algorithms reported the same ξ value for the Fast Fourier and Welch methods. Fast Fourier Transform had better convergence with the Levenberg-Marquardt method, while Welch method had better convergence with the trust-region-reflective method. Taken together, these results suggest that the SBI method can be practically implemented on short to medium span bridge girders under operational conditions for in-service structural assessment and load rating.

4. Concluding Remarks

This study was set out to assess the feasibility of using the proposed SBI method for structural assessment of existing beam-like structures. Numerical and experimental studies were carried out for beams with different configurations, boundary conditions, and various sources of excitation. In most case studies, stiffness and boundary condition were accurately estimated, and the corresponding capacity was evaluated using structural index and live load ratio. For more complex structures such as the box girder herein, the accuracy of the results is improved by placing sensors at the locations that are more suitable to estimate bending mode such as the top flange. In this case, conducting modal analysis with different sensor layouts will be helpful to determine such positions. The key strengths of the SBI method are that no initial numerical model and prior information on support condition are required. The testing setup of the SBI method is suitable for short to medium span bridges to assist in the decision-making process for higher order assessment.

5. Acknowledgment

6. References

1.   Y. B. Yang and J. P. Yang, State-of-the-art review on modal identification and damage detection of bridges by moving test vehicles, *Int. J. Struct. Stab. Dyn.* **18** (2018) 1-31.

2.   S. Jamali S, T.H.T. Chan, D. P. Thambiratnam, R. Pritchard and A. Nguyen, Pre-test finite element modelling of box girder overpass-application for bridge condition assessment, in *Proc. Australasian Structural Engineering Conf. (ASEC),* Brisbane, Australia (2016), pp.1-8.

3.   Y. B. Yang Y, B. Zhang, Y. Qian and Y. Wu, Contact-point response for modal identification of bridges by a moving test vehicle, *Int. J. Struct. Stab. Dyn.* **18** (2018) 1850073.

4.   Bridge Design- Part 7: Bridge Assessment (AS 5100.7), Sydney, Australia (2017).

5.   J. Brownjohn, F. Magalhaes, E. Caetano and A. Cunha, Ambient vibration re-testing and operational modal analysis of the Humber Bridge, *Eng. Struct.* **32** (2010) 2003-2018.

6.   E. P. Carden and P. Fanning, Vibration based condition monitoring: a review, *Struct. Health Monit* **3** (2004) 355-377.

7.   S. Hoffmann, R. Wendner, A. Strauss and K. Bergmeister, Comparison of stiffness identification methods for reinforced concrete structures, *6th Int. Workshop on Structural Health Monitoring: Quantification, Validation, and Implementation*. Stanford, California 2007.

8.   H. Subramaniam, A non-destructive method for determining the adequacy of in-service corbelled timber girder bridges, *17th ARRB Conf.* Gold Coast, Queensland (1994), pp. 103-119.

9.   M. R. Chowdhury, Rapid beam load capacity assessment using dynamic measurements (Research Structural Engineering, Vicksburg, 1999).

10.   N. Haritos, F. Rapattoni, J. Howell, J. Higgs, G. L. Hutchinson, A. Giufre and D. Tongue, Load capacity of in-service bridges, in *Proc. Austroads Bridges Conf.* Brisbane, Australia (1991), pp. 277-288.

11.   J. Higgs and D. Tongue, Dynamic Bridge Testing Systems (DBTS) for the evaluation of defects and load carrying capacity of in-services bridges. *Int. Conf. on Current and Future Trends in Bridge Design Construction and Maintenance,* Singapore (1999), pp. 1-21.

12.   P. Siswobusono, S-E. Chen, S. Jones S, D. Callahan, T. Grimes and N. Delatte, Serviceability-based dynamic loan rating of a LT20 bridge, *Experimental Tech.* **28** (2004) 33-36.

13.   X. Wang, J.P. Wacker, A. M. Morison, J. Forsman, J. Erickson and R. Ross, *Nondestructive assessment of single-span timber bridges using a vibration-based method* (USDA Forest Service, Washington, 2005).

14.   A.K.M.A. Islam, A. S. Jaroo and F. Li, Bridge load rating using dynamic response, *J. Perform. Constr. Faci.* **29** (2014) 1-11.

15.   W. Ariyaratn, B. Samali, Li J, K. Crews, M. Al-Dawod, Development of a cost-effective load assessment technique for slab and P-unit type bridge decks. *6th Austroad Bridge Conf.* Perth, Australia (2006), pp.1-14.

16.   S. Jamali, K. Y. Koo, T. H. T. Chan, A. Nguyen and D. P. Thambiratnam, Assessment of Flexural Stiffness and Load Carrying Capacity Using Substructural System. in *Proc. Int. Conf. on Structural Health Monitoring of Intelligent Infrastructure (SHMII-08)*, Brisbane, Australia (2017), pp.1-11.

17.   C. Koh, B. Hong and C. Liaw , Substructural and progressive structural identification methods, *Eng. Struct.* **25** (2003) 1551-1563.

18.   C. Koh and K. Shankar, Substructural identification method without interface measurement, *J. Eng. Mech.* **129** (2003) 769-776.

19.   D. Zhang, *Controlled substructure identification for shear structures*, PhD thesis, University of Southern California, California (2010).

20.   C. G. Koh, L. M. See and T. Balendra, Estimation of structural parameters in time domain: a substructure approach, *Earthquake Eng. Struct. Dyn.* **20** (1991) 787-801.

21.	N. Lakshmanan, B. Baghuprasad, K. Muthumani, N. Gopalakrishnan and D. Basu, Identification of reinforced concrete beam-like structures subjected to distributed damage from experimental static measurements, *Comput. Conc.* **5** (2008) 37-60.

22.	M. Paz, *Structural dynamics: theory and computation* (Van Nostrand Reinhold, New York, 2012).

23.	R. Blevins, *Formulas for natural frequency and mode shape* (Van Nostrand Reinhold, New York, 1979).

24.	B. Bakht and L. G. Jaeger, *Bridge analysis simplified* (McGraw-Hill, New York, 1985).

25.	J. Billing, *Estimation of the natural frequencies of continuous multi-span bridges* (Ministry of Transportation and Communications, Ontario, 1979).

26.	Bridge Design- Part 2: Design Loads (AS 5100.2), Sydney, Australia (2017).

27.	H. Moravej, S. Jamali, T. H. T. Chan and A. Nguyen, Finite Element Model Updating of civil engineering infrastructures: a review literature. in *Proc. Int. Conf. on Structural Health Monitoring of Intelligent Infrastructure*, Brisbane, Australia (2017), pp. 1-12.

28.	Queensland Department of Transport and Main Roads (TMR), *Tier 1 Bridge Heavy Load Assessment Criteria* (Queensland, Australia, 2013).

29.	T. H. T. Chan and D. P. Thambiratnam, *Structural Health Monitoring in Australia* (Nova Science Publishers, New York, 2014).

30.	L. R. Rabiner and B. Gold, *Theory and application of digital signal processing* (Prentice-Hall, Englewood Cliffs, 1975).

31.	T. F. Coleman and Y. Li , An interior trust region approach for nonlinear minimization subject to bounds, *SIAM J. Optim.* **6** (1996) 418-445.

32.	J. J. Moré, The Levenberg-Marquardt algorithm: implementation and theory, in *Conf. on Numeical Analysis,* Heidelberg, Berlin (1977), pp. 105-116.